Recent Sedimentation of a Mesotidal Wave-Dominated River Mouth

Chien, Nguyen; Tung, Tran Thanh

Published in:
Journal of Coastal Research

DOI:
10.2112/SI81-007.1

Publication date:
2018

Citation for published version (APA):
Chien, N., & Tung, T. T. (2018). Recent Sedimentation of a Mesotidal Wave-Dominated River Mouth: Lach Van, Vietnam. *Journal of Coastal Research*, *81*(sp1), 50-56. https://doi.org/10.2112/SI81-007.1

Recent Sedimentation of a Mesotidal Wave-Dominated River Mouth: Lach Van, Vietnam

Nguyen Q. Chien[†*] and Tran T. Tung[†‡]

[†]Division of Marine and Coastal Management, Water Resources (Thuyloi) University, Hanoi 116705, Vietnam.

[‡]Institute of Construction Engineering, Water Resources (Thuyloi) University, Hanoi 116705, Vietnam.

ABSTRACT

The sedimentation of a wave-dominated river mouth in Tonkin Gulf, Vietnam, has been investigated for the time period 2005–2017. Deepwater wave statistics and the corresponding potential longshore transport (LST) has been determined, which shows a net LST rate of ~10^5 m^3/yr southward. A one-line model is used to estimate the change in local coastline; the model is verified against shoreline position data obtained from satellite images. It is apparent that the accretion occurs on both sides of the river mouth with a rate of ~10 m/yr. Coastline evolution trend is then predicted for the aforementioned time period, and it is evident that accretion intensifies in recently, which is most probably due to slight variation in local wave climate. Results of this study can be used as a scientific basis to propose solutions for stabilizing the river mouth entrance and its channel.

ADDITIONAL INDEX WORDS: *Sedimentation, wave climate, river discharge, longshore sediment transport, satellite image.*

INTRODUCTION

The morphology of typical wave-dominated river mouths has been extensively discussed (Wright, 1977; Carter, 1988; Woodroffe, 2001). Recently increasing attempts (Warner *et al.*, 2008; Pinto *et al.*, 2012; Guérin *et al.*, 2016) have been made to quantify the change in bathymetry of this particular type of coastal system, with mathematical modeling as an essential tool. Nevertheless, coastal sediment transport and deposition remain too complex to be determined accurately. Contemporary researches usually integrate descriptive aspects in classical geomorphology with numerical computations to predict interesting features of shoreline patterns (Dan *et al.*, 2011; Hoan *et al.*, 2011; Nardin and Fagherazzi, 2012; Nienhuis *et al.*, 2016). Basically, two types of numerical models are used: coastline model where the position of shoreline is tracked during simulation time period, and coastal area model, where bathymetry of the surf zone area is tracked and the shoreline is interpolated on the bathymetry as the isoline at the mean water level. The latter provides more details, but requires comprehensive dataset, especially bathymetric data; whereas the former is essentially one-dimensional

and required only a representative beach profile in addition to the coastline planform. It has been shown that improved versions of coastline model can handle highly convoluted planforms (Ashton and Murray, 2006; Hurst *et al.*, 2015).

Predicting the change in coastline has become an essential task in coastal management for many nations. Shoreline may exhibit either erosion or accretion. While the former is a frequently alerted issue in Vietnam, estuarine sedimentation is another problem of concern to local inhabitants. Along the coast of Vietnam, a number of fishing ports are in operation to serve the food demand. The Lach Van port is one such port in Nghe An Province, which is dedicated for fishing but also acts as a shelter for vessels against storms since 2003. However, in recent years the natural channel leading to this port is frequently accreted. As local fishing vessels are growing in both size and power, navigation through the channel is difficult and unsafe. According to the Lach Van port authority, annually there are about eight vessels grounded, affecting the local fishery. Hence, timely identification of the cause for sedimentation also helps in designing efficient countermeasures.

The aim of this research is to investigate the sediment accretion process at Lach Van river mouth. The study incorporates an evaluation on sediment budget of the coastal system. A one-line numerical model is utilized to simulate the accretion process, with verification and sensitivity analysis being carried out. The study attempts to reveal key factors contributing to sedimentation, given the lack of detailed surveyed data as in most preliminary phases of coastal projects for developing countries.

STUDY AREA AND LITTORAL PROCESSES

The Lach Van river mouth (18.98°N, 105.62°E) in Vietnam is the interface of a small river (Bung) to Dien Chau bay, part of Tonkin Gulf (Figure 1). The river cuts through the middle section of a concave coast (~24 km long), bounded by two rocky headlands. The average depth of the enclosed bay is ~7 m. Geological research by Hong and Thoa (2007) showed that this coast is mainly formed by mixed sediment of river and sea. Along the coastline, beach strands are separated by rocky headlands. The typical geological processes are deposition and abrassion of sediment. Marine bedform contains ripples and small sand dunes. Minor ridges present within the breaker zone.

On the two sides of the estuary, the northern shoreline is more curved and the beach profile relatively milder, with finer sediment grains. The southern shoreline is more straight and beach profile more steeply sloped. This crenulate-shaped coastline suggests dominant ENE swell waves. Hsu and Evans' (1989) formula for parabolic coastline model is apparently applicable for the local coastline, with characteristic angle $\beta = 32°$, control line length $R_0 = 21.2$ km and a corresponding schematized equation for the radius: $R/R_0 = 0.041 + 1.166(\beta/\theta) - 0.210(\beta/\theta)^2$; this is found to be quite valid for the local coast within the range $\beta \leq \theta \leq 145°$.

The tidal regime is nonuniformly diurnal. The tidal range is TR = 1.2–2.5 m. For the annually average wave properties $H_s = 0.5$ m; $T = 3.6$ s (Hung and Dien, 2009), the relative magnitudes

between H_s and TR suggest that coastal system falls into the "mixed energy (wave-dominated)" category (Hayes, 1979). More specifically, with a Dean number $\Omega \sim 18$, the beach can be classified as "dissipative" to wave actions (Wright and Short, 1984).

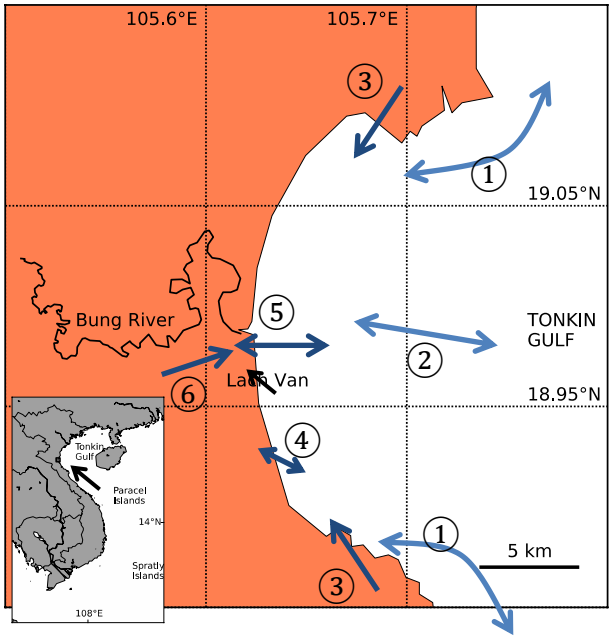

Figure 1. Location of the study area, with basic modes of sediment transport (see explanation in the text)

Based on the above geographical settings, hydrodynamic, topographic and geological conditions, it can be seen that coastal sediment tends to move in several modes as depicted in Figure 1. The long-shore current is responsible for transporting suspended sediment ① around rocky headlands (Goda, 2010). The embayed beach can be supplied by sediment from the erosion of headland ③ especially under wave action. However, this source is relatively minor as erosion rate for local limestone rock is typically 1 mm/yr, yielding just 10 m^3 sediment from each headland annually, assuming that erosion takes place along the entire periphery of the headland. Cross-shore sediment transport components, including the wave-induced ②, wind-induced ④, and tidal-induced ⑤, are considered to produce zero net flow over a long time, in order to maintain an equilibrium profile for the beach.

Previous studies hardly provided any estimations on the total longshore transport (LST) for the area, possibly because research efforts have been prioritized to areas being prone to erosion in Vietnam. For a larger coastal area (18°N to 19.5°N), Hong and Thoa (2007) quoted a net LST of 1.94×10^6 m^3/yr southward. In another study (Tien, 2004) for an embayed coast (17.8°N) with similar planform and orientation, the net LST was estimated to be 1.0×10^6–1.5×10^6 m^3/yr (northward).

The flow from river Bung (48 km long, basin area 738 km^2) is relatively weak, though infrequently intense river floods are expected to supply sediment to the estuary ⑥. Based on typical relationships between basin area and river discharge properties presented by Milliman and Syvitski (1992), the sediment yield for this river basin (belonging to 'lowland/coastal plain' category) is likely in the range of 10^7–6×10^7 kg/yr, or 6.3×10^3–3.8×10^4 m^3/yr, assuming a sediment porosity of 0.4.

Apparently the LST component is the key factor to sediment accretion in the estuary. Estimation of LST with shoreline change is presented Section 4 (shoreline modeling).

DATA COLLECTION

To evaluate the intensity of sediment deposition over time, it is first necessary to identify the variation in wave climate offshore the study area. Wave time-series data for the deepwater location 19°N, 106°E during 2005–2017 has been collected from NOAA WaveWatch III archive (NOAA, 2017). By partitioning the available data into two 6-year periods, it can be seen (Figure 2) that dominant wave directions sorted by influence are ENE > ESE ≈ NE > SE. Also, the latter period witnessed a slight decline of ENE waves and minor intensification of NE waves.

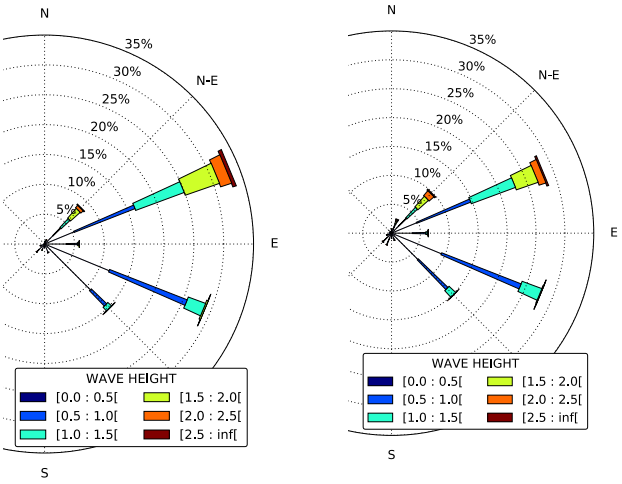

Figure 2. Wave roses of the periods Feb-2005 – Jan-2011 (left) and Feb-2011 – Jan-2017 (right)

For each direction, it is possible to estimate a morphological wave height, H_{mor}, which is representative for long-term change of the coastline (De Vriend *et al.*, 1993):

$$H_{mor} = \left(\frac{\sum P_i H_i^n}{\sum P_i} \right)^{1/n} \quad (1)$$

A value $n = 2.5$, which is consistent with the CERC formula and widely applied in practice, is used (Roelvink and Reniers, 2011). To evaluate the representative wave period T_p, an empirical correlation between H_s and T_p is needed. Linh and Tuan (2015) derived separated formulas to calculate T_p for either NE or SW monsoon. However for inter-annual simulations in this study, it is more reasonable to choose one common formula for T_p.

Based on the data extracted for period 2011–2017 (Figure 3), it is possible to discern sea waves and swell; the former is more pervalent among high waves and is thus more relevant to shaping the shore. Here a criterion based on deep-water wave steepness $s_0 = H_s/1.56T_p^2 = 0.01$ is used for separation purpose. For the sea waves, a relationship $T_p = 5.06H_s^{0.5}$ is adopted.

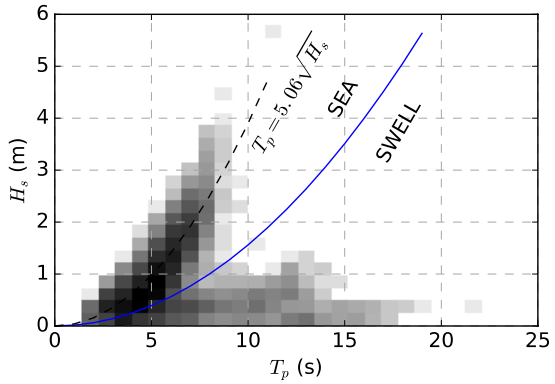

Figure 3. Relationship between wave height and peak period; separation between wind seas and swells is indicated. (Color shades shows density of the data points.)

The average wave steepness chosen for wind seas is 0.025, from which wave periods corresponding to H_{mor} are calculated, for further use in Section 4 (shoreline modeling).

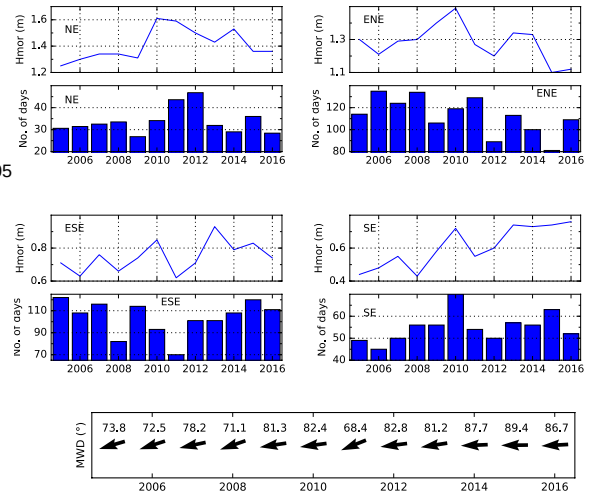

Figure 4. Trend of deep-water characteristic waves

The annual trend of wave dominance (both wave height and occurrence) for major wave directions (NE, ENE, ESE, and SE) are shown in Figure 4. Also shown is the trend in mean wave direction (here only wave heights ≥ 0.75 m are considered). It can be seen that in long term, ESE and SE waves slightly increases while ENE waves decreases. A long-term change in wave direction is identified with increasing contributions from ESE and SE waves.

Among the collection of surveyed profiles along Vietnam coast (MARD, 2012), the #23 profile (105.624°E, 19.018°N) is chosen. The profile is located on the northern side, 4 km from the inlet, with a nearshore beach slope of 3‰ and a profile-average slope of 0.9‰. The seabed elevations are consistent with those obtained from SRTM30 and GEBCO-2014 data sources (Becker *et al.*, 2009; Weatherall *et al.*, 2015) (Figure 5). Another measured profile of a smaller bay southward (18.837°N, 105.716°E) exhibits steeper nearshore slope (8.4‰). On a local map scaled 1:50,000, the slope of nearshore profile (from shoreline down to 3-m depth contour) varies from 3‰ to 5‰. A representative bedslope for the coast is taken as 5‰.

Comparing to a conventional Bruun-Dean profile, the sediment grain size D_{50} is likely ~ 0.1 mm for the steep southern part of the bay, and ~0.05 mm (silt type) for the coastal part near the river mouth. Field surveys reported by Sao *et al.* (2010) for another site (107.1°E, 17.0°N), with similar geological setting, also showed the pervalence of fine sediment (grain size < 0.1 mm) in the surf zone near a river mouth.

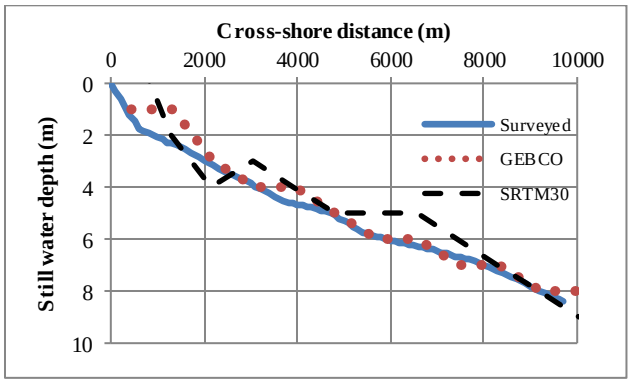

Figure 5. Beach profile (location 105.624°E, 19.018°N)

On satellite image (Google, 2017a) the coast shows various shore-parallel contour lines in distinct shades, which implies progressive accretion and intrusion of marine sediment into the estuary. The latter is remarkably visible from sand deposition at the groin field in the southern bank of the estuary (also see the map inset on Figure 6).

Synthetic aperture radar (SAR) images of interferometric wide swath (IW) type (resolution 20 m × 22 m; pixel spacing 10 m × 10 m) have been collected from Sentinel-1 satellite (European Space Agency, 2017) for the study area. The image dates are 28-Mar-2015, 15-Feb-2016 and 12-Oct-2016 (intentionally chosen during calm condition to avoid temporary changes in beach profile due to storm events), at appropriate times such that the local water level was about mean tidal level (with variation $\leq \sim 10$ cm). Higher-resolution airborne images dated 19-Sep-2009, 5-Aug-2011, 31-Aug-2011, and 30-May-2014, in Google Earth (Google, 2017b) have also been retrieved for close inspection of the river mouth; however the exact times of these images, hence the water level, are uncertain.

The shorelines are then digitized and shown in Figure 6. It can be seen that the change in shoreline position is mostly pronounced in northern beach of the river mouth. Over ~1.5 years since Mar-2015, subtle changes in shoreline position (~20 m) can be identified. However, distance errors might emerge during image rectification, and changes in water level; the latter might be up to 10 m, assuming a beach face slope of 0.01 corresponding to fine sand composition. The upper map inset presents a zoom-in of the river mouth during 2015–2016, from which the northern sand spit tended to curve inward and the part of beach sediment tends to be transported toward the mouth.

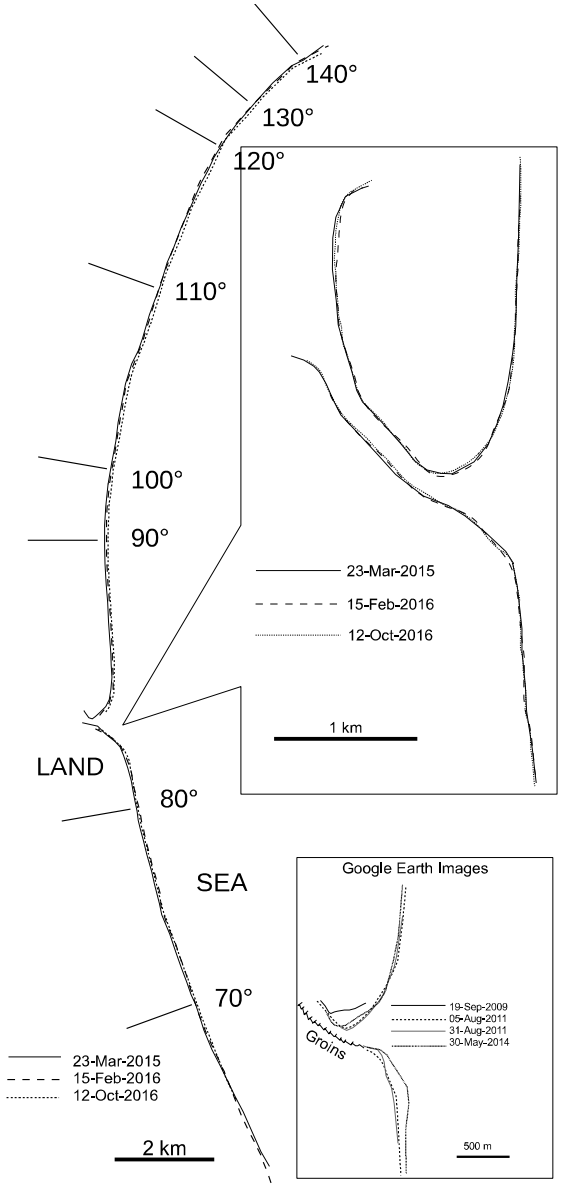

Figure 6. Shorelines of the study area on various dates. Text annotations e.g. 130°, 120° indicate shoreline orientation.

155

From the lower small map inset (compiled from Google Images), the northern sand spit tends to move landward whereas the southern coast shows a trend of expanding, however the exact position of shoreline is questionable, as the newly accreted area is shallow and gently sloped. The 30-May-2014 shoreline might be too advanced, probably because the airborne image was taken during low
160 water.

SHORELINE MODELING

With extensive data on shoreline shape and position but limited data regarding bathymetry, an appropriate method is using one-line models, whose mathematical foundation was derived by Pelnard-Considère (1956). Various one-line models have emerged, including GENESIS (Hanson and Kraus, 1989), ONELINE (Dabees and Kamphuis, 1998), LITPACK (Danish Hydraulic Institute, 2003) and UNIBEST (developed by Deltares, formerly Delft Hydraulics), among others. In this paper, the Generic Coastline Model (GCLM) by Roelvink and Reniers (2011) is used with proper modifications to the codebase in order to implement various LST formulas, and to assess the influence of the river to coastline dynamics.

Similar to UNIBEST, in GCLM, the coastline is approximated as a cubic spline, and for the present study, is divided into 120 segments of length Δx = 220 m.

In calculating the LST rate (Q_L, m^3/yr.), three popular bulk-type formulas: Kamphuis (1991), Van Rijn (2014), and Bayram *et al.* (2007), are used besides Soulsby–Van Rijn formula (Soulsby, 1997). The first one, Eq. (2), was improved by Schoonees and Theron (1996) for open coast and fine sand. The last one, Eq. (5), gives the transport rate through each meter section of the profile, and must be integrated over the surf zone to yield Q_L. To obtain the cross-shore distribution of H_s and longshore velocity, v, a non-uniform grid with spacing 2–50 m is used.

$$Q_L = 89594 H_b^2 T_p^{1.5} D_{50}^{-0.25} (\tan\beta)^{0.75} (\sin 2\alpha_b)^{0.6} \quad (2)$$

$$Q_L = 31339 K_{swell} D_{50}^{-0.6} (\tan\beta)^{0.4} H_b^{2.6} V_L \quad (3)$$

$$Q_L = \frac{\varepsilon (E c_g \cos\alpha)_b V_L}{(\rho_s - \rho) g w_s (1 - p)} \quad (4)$$

$$q = C_{sv} (A_b + A_s) v x \quad (5)$$

The transport coefficient in Eq. (4) is $\varepsilon = (4 + 9H_b/w_s T_p)\times 10^{-5}$. The calibration factor C_{sv} is initially set as 0.04. Other coefficients appearing in Equations (2–5) can be found in corresponding references. The wave breaking index γ is dependent on the deepwater wave steepness: $\gamma = 0.5 + 0.4\tanh(33 s_0)$ (Battjes and Stive, 1985).

Other sediment-related parameters include: grain size D_{50} = 0.1 mm (correspondingly, the fall velocity w_s = 0.0078 m/s), D_{90} = 0.2 mm, and porosity p = 0.4. These parameter values serve as a base scenario for modeling.

Judgement on shoreline change can be made only after specifying an active profile height ($B + h_*$). Along the local coastline, where the beach consists of fine sand, a typical berm height $B \sim 0.5$ m is observed. The closure depth, h_*, on the other hand, can be estimated through an empirical formula (Hallermeier, 1981):

$$h_* = \left(\bar{H}_s - 0.3\,s\right)\bar{T}_s\sqrt{\frac{g}{5000\,D_{50}}} \quad (6)$$

For the wave dataset obtained the average significant wave height, $\bar{H}_s$ = 0.792 m (correspondingly, $\bar{T}_s$ = 4.5 s), standard deviation of wave height variability, σ = 0.538 m, yielding h_* = 12.6 m.

The coastline evolution is governed by the sediment balance:

$$\frac{\partial y}{\partial t} + \frac{1}{B + h_*}\left[\frac{\partial Q_L}{\partial x} - q\right] = 0 \quad (7)$$

The sediment source or sink, q, is omitted for open coasts in which zero net cross-shore transport. At the river mouth, however, a permanent source of sediment exists. The yearly sediment flux, ~10^4 m^3, is assumed to be distributed over ~400 m of the gap width, yielding q ~ 25 m^2/yr. In practice, however, it is more convenient to supply a sediment flux of q/2 for each of the coastal cell adjacent to the gap.

The simulation time starts from 23-Mar-2015, with a time step of 0.02 yr, in order to achieve numerical stablity for the explicit scheme. Two simulated shoreline positions are extracted (15-Feb-2016 and 12-Oct-2016, corresponding to durations of ~10.5 months and 18.5 months) and compared with observed data.

RESULTS AND DISCUSSIONS

Before analysing shoreline change, the LST variation along the coast is considered. As the shoreline is concave with orientation gradually varying from 140° to 70° (north to south), LST rate is examined for each shoreline segment with orientation differentiated by ±10°. The results are shown in Table 1, where the potential LST (in 10^5 m^3/yr.) is positive for southward transport and negative for northward transport. Simulation 1 ends on 15-Feb-2016 and the successive simulation 2, on 12-Oct-2016.

Table 1. Potential net LST (×10^5 m^3/yr.)

	Sim. 1				Sim. 2			
Ori.	KH	VR	BR	SVR	KH	VR	BR	SVR
140°	1.14	1.30	2.59	2.34	0.98	1.22	2.62	1.69
130°	1.42	1.80	3.60	2.29	1.04	1.34	2.96	1.54
120°	1.55	2.41	5.21	2.38	0.92	1.55	3.73	1.19
110°	1.70	2.93	6.97	2.59	0.79	1.60	4.29	0.92

100°	1.84	3.21	8.28	2.42	0.65	1.37	4.11	0.72
90°	1.81	3.08	8.55	2.13	0.47	0.94	3.25	0.52
80°	1.56	2.49	7.36	1.72	0.18	0.33	1.71	0.30
70°	0.97	1.46	4.67	1.06	–0.29	–0.41	-0.41	0.06

Note: Ori. = shoreline orientation, as shown in Figure 6; formula abbreviations: KH = Kamphuis, VR = Van Rijn, BR = Bayram, SVR = Soulsby–Van Rijn.

All formulas yield the main LST direction being southward. Simulation 2 exhibits a marked difference with negative LST rate in the southern part of the coast. The reason is simulation 2 lasts for less than a full year (lacking of winter when the local NE monsoon is dominant), consequently the southward transport is weakened.

The computed LST direction is in agreement with intuition. At the southmost point of the crenulate bay, the net LST is almost zero, indicating a 'null-point' where the shoreline tends to align parallel to the predominant or 'mean wave' crests. For bays facing moderately open seas with slight coastline concavity and identation such as the study area, the pattern of sediment transport may be from headlands to the middle, as suggested by Goda (2010).

The Van Rijn formula, in certain cases, produces a LST rate twice larger than that of Kamphuis formula. In the latter, Q_L is proportional to H_b^2 instead of $H_b^{2.6}$ in the former. Also, the former takes into account for occasional swell waves, which is expected to be responsible for an increase of 10% of LST (Van Rijn, 2014).

The Bayram formula generally produces largest LST rate, due to its direct (reciprocal) dependence on sediment fall velocity. In fact, for fine sand, halving the D_{50} would reduce w_s by over 3 times, which greatly increase Q_L. This constrasts to the weaker dependence on D_{50} of the Kamphuis and Van Rijn formulas (with proportional powers of 0.25 and 0.6, respectively).

The Van Rijn formula gives intermediate value range for LST rates, and closer to Kamphuis formula. The former also approximates the integrated LST from cross-shore distribution of local transport rate obtained via Soulsby–Van Rijn formula; and can be used as a reference basis in calculating shoreline change.

In two simulations for shoreline change, the active profile heights are $B + h_* = 13.1$ m for Simulation 1 and 10.8 m for Simulation 2. The river mouth gap is assigned to four consecutive cells, #57–#60, which is wider than the actual one. This is necessary, as the coastline must be modeled as a smooth curve and the sharply indented part of natural shoreline is omitted.

The shoreline positions at the end of these simulations are shown on Figure 7. There is a noticeable trend of accretion immediately on both sides of the inlet. The shoreline advancement is more

apparent on the left side, with continual sand supply from LST. Certain details in shoreline change pattern are similar to those from observed data: the accretion on the northern side and erosion in southern downdrift side is captured. The distance difference between simulated and measured might be up to 10 m.

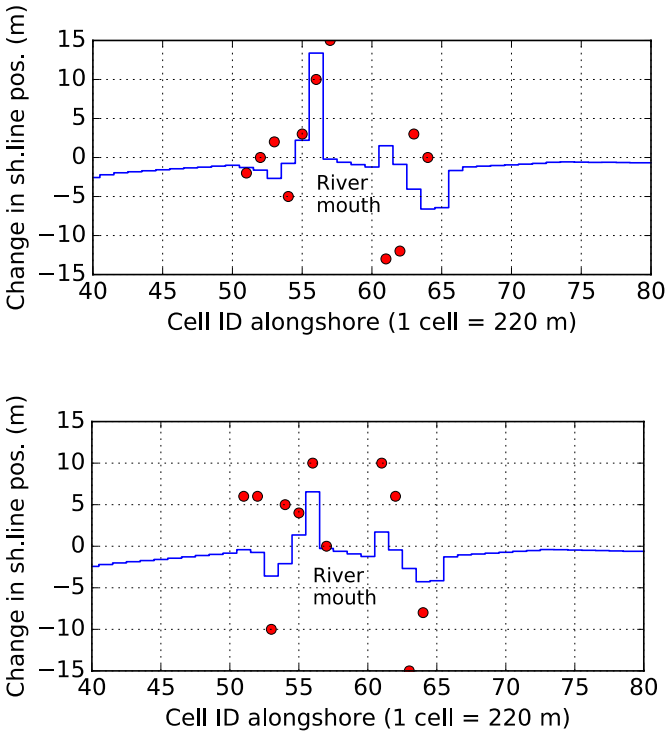

Figure 7. Change in shoreline positions after simulations 1 (upper) and 2 (lower) in comparison with observed data

Due to the freshwater outflow, part of the longshore sediment is trapped. The volume of deposited material, V, on a first estimate, is related to the gross LST arriving at either side of the gap; $V = 4.5\times10^4$ m^3 for simulation 1, and 1.9×10^4 m^3 for simulation 2. Through sensitivity analysis, it is shown that typical uncertainty of the input parameters listed in Table 2 (Soulsby, 1997), the respective change in V (with regard to the base scenario). The variation in shoreline position (y_{max}) is generally larger than that of accretion volume. Sediment input from river also has influence on the change of river mouth, although this influence is not clearly shown in terms of accretion volume.

Table 2. Sensitivity of result to parameters

Parameter	Range	ΔV	Δy_{max}
Wave height, H_s	±10%	41%	41%
Wave period, T_p	±10%	7.5%	18%
Wave direction, θ	±15°	13%	22%
Grain size, D_{50}	±15%	10%	13%
Depth, h	±10%	4.0%	5.3%
Sed. source (river)	–50%	0.0%	10%

A simulation for predicting coastline evolution near the river mouth during the years 2005–2017 is performed. The result is shown on Figure 8, where apparently the year 2011 witnessed most pronounced change in shoreline position.

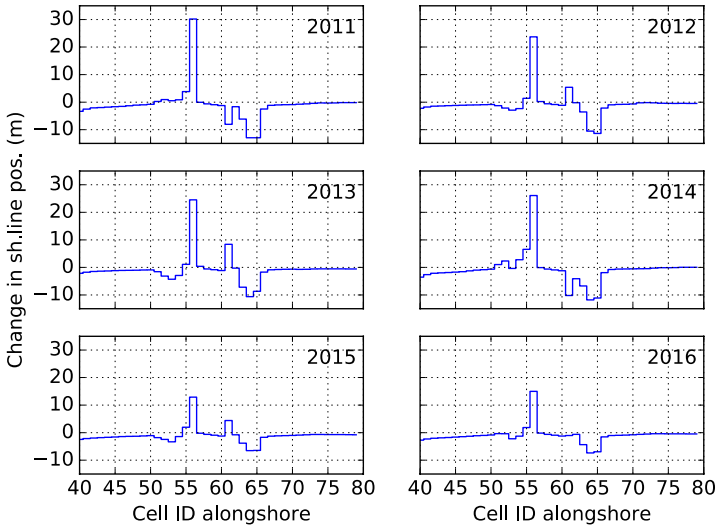

Figure 8. Yearly changes in shoreline position

Cross-shore sand transport may be responsible for the loss of sand budget. Donnelly *et al.* (2004), in studying the erosion of Hai Hau beach (Vietnam), postulated that the amount of sediment loss on a straight coast adjacent to a river mouth is related to the difference in equilibrium profile area between the delta and the coast. However, this is not evident in the present study, as the typical profile (Figure 5) is gently sloped, without any obvious tendency of cross-shore erosion.

The sediment supply through the northern boundary may be significant due to a large potential LST of the adjacent pocket beach to the north (coastline orientation ~90°), however because of the abrupt change in shoreline orientation across the northern headland, a sharp decrease in local LST rate is expected, and most of this sediment source should settle at this end of the bay.

CONCLUSIONS

For Lach Van river mouth, the basic cause for sedimentation is due to waves causing longshore current bringing sediment accretes at the river mouth. Calculation shows that the local potential net LST mostly directs southward with a rate of ~10^5 m^3/yr. This rate has decreased during the years 2011–2016, as apparent from the calculated annual shoreline changes during this period. If this amount of sediment (~10^5 m^3/yr) is completely deposited then accretion at the river mouth (area~1 km^2) will occur at a rate of ~10 cm/yr. Analysis of sediment process at the Lach Van river mouth can be used as a scientific basis to design stabilization measure for the entrance and its channel.

The use of a one-line model for this study has certain drawbacks: the shoreline orientation at the river mouth is not accurate, hence the simulated change in coastline is not well represented. The assumption of an identical beach profile shape along the coast leads to errors in LST calculation. However, this approach is justifiable in the context of inadequate data, especially regarding bathymetry and fluvial sediment load. In further design of construction works, the shoreline dynamics should be assessed using a 2-D depth-averaged model.

The river outflow seems to play a minor role in local shoreline change, though infrequent river floods should causes short-term changes of the coastline.

ACKNOWLEDGMENTS

The study is funded by a research grant from the University of Water Resources (Thuyloi), Vietnam.

LITERATURE CITED

Ashton, A.D., and Murray, A.B., 2006. High-angle wave instability and emergent shoreline shapes: 1. Modeling of sand waves, flying spits, and capes. *Journal of Geophysical Research: Earth Surface*, 111, F04011.

Bayram, A.; Larson, M., and Hanson, H., 2007. A new formula for the total longshore sediment transport rate. *Coastal Engineering*, 54(9), 700–710.

Battjes, J.A., and Stive, M.J.F., 1985. Calibration and verification of a dissipation model for random breaking waves. *Journal of Geophysical Research*, 90(C5), 9159–9167.

Becker, J.J.; Sandwell, D.T.; Smith, W.H.F.; Braud, J.; Binder, B.; Depner, J.; Fabre, D.; Factor, J.; Ingalls, S.; Kim, S-H.; Ladner, R.; Marks, K.; Nelson, S.; Pharaoh, A.; Trimmer, R.; Von Rosenberg, J.; Wallace, G., and Weatherall, P., 2009. Global bathymetry and elevation data at 30 arc-seconds resolution: SRTM30_PLUS. *Marine Geodesy*, 32(4), 355–371.

Carter, R.W.G., 1988. Coastal Environments: an Introduction to the Physical, Ecological and Cultural System of Coastlines, Academic Press, 617p.

Dabees, M., and Kamphuis, J.W., 1998. ONELINE, a numerical model for shoreline change. *Proceedings of 26th International Conference on Coastal Engineering*, (Copenhagen, Denmark), 2668–2681.

Dan, S.; Walstra, D.-J.R.; Stive, M.J.F., and Panin, N., 2011. Processes controlling the development of a river mouth spit, *Marine Geology*, 280, 116–129.

Danish Hydraulic Institute, 2003. An integrated modeling system for littoral processes and coastline kinetics. *Short Introduction and Tutorial*.

De Vriend, H.J.; Capobianco, M.; Chesher, T.; De Swart, H.E.; Latteux, B., and Stive, M.J.F., 1993. Approaches to long-term modelling of coastal morphology: a review. *Coastal Engineering*, 21, 225–269.

Donnelly, C.; Hung, N.M.; Larson, M., and Hanson, H., 2005. One-line modelling of complex beach conditions: An application to coastal erosion at Hai Hau beach in the Red River Delta, Vietnam. In: *Proceedings of the 29th Conference on Coastal Engineering* (Lisbon, Portugal), pp. 2449–2461.

European Space Agency (ESA), 2017. Copernicus Open Access Hub, https://scihub.copernicus.eu

Goda, Y., 2010. *Random Seas and Design of Maritime Structures*, 3rd Edition, Singapore: World Scientific, 732p.

Google, 2017a. *Map of Dien Chau District, Nghe An, Vietnam*. Imagery © 2017 CNES/Airbus, DigitalGlobe. Available from http://bit.ly/2txIZ3W.

Google, 2017b. Google Earth. Image © 2017 DigitalGlobe. Lat. 18.982, lon. 105.621, eye alt. 13894 ft.

Guérin, T.; Bertin, X., and Dodet, G., 2016. A numerical scheme for coastal morphodynamic modelling on unstructured grids. *Ocean Modelling*, 104, 45–53.

Hallermeier, R.J., 1981. A profile zonation for seasonal sand beaches from wave climate, *Coastal Engineering*, 4, 253-277.

Hanson, H., and Kraus, N.C., 1989. GENESIS: Generalized model for simulating shoreline change. CERC Report 89-19, US Corps of Engineers, Vicksburg.

Hayes, M.O., 1979. Barrier island morphology as a function of tidal and wave regime. *In*: S. Leatherman (ed.), *Barrier Islands from the Gulf of St Lawrence to the Gulf of New Mexico*. New York: Academic Press, pp. 1–27.

Hoan, L.X.; Hanson, H.; Larson, M., and Nam, P.T., 2011. Modeling regional sediment transport and shoreline response in the vicinity of tidal inlets on the Long Island coast, United States, *Coastal Engineering*, 56(6), 554–561.

Hong, L.X., and Thoa, L.T.K., 2007. *Coastal Geomorphology of Vietnam* (in Vietnamese), Vietnam: Publishing House for Science and Technology, 278p.

Hsu, J.R.C., and Evans, C., 1989. Parabolic bay shapes and applications. *Proceedings of the Institute of Civil Engineers*, 87(4), 557–570.

Hung, N.M., and Dien, D.C., 2009. *Wave Energy of South China Sea and Along the Coast of Vietnam* (in Vietnamese), Hanoi: Publishing House for Science and Technology, 330p.

Hurst, M.D.; Barkwith, A.; Ellis, M.A.; Thomas, C.W., and Murray, A.B., 2015. Exploring the sensitivities of crenulate bay shorelines to wave climates using a new vector-based one-line model. *Journal Geophysical Research: Earth Surface*, 120, 2586–2608.

Kamphuis, J.W., 1991. Alongshore sediment transport rate. *Journal of Waterway, Port, Coastal and Ocean Engineering*, 117, 624–640.

Linh, D.T., and Tuan, T.Q., 2015. Establishment of a relationship between wave period and height for Northern and North-Central coasts of Vietnam (in Vietnamese). *Proceedings of Annual Conference on Water Resources*, pp407–409.

MARD (Vietnamese Ministry of Agriculture and Rural Development), 2012. *Technical Guidelines for Sea-Dike Design*, in Vietnamese.

Milliman, J.D., and Syvitski, J.P.M., 1992. Geomorphic/tectonic control of sediment discharge to the ocean: the importance of small mountainous rivers. *Journal of Geology*, 100, 525-544.

Nardin, W., and Fagherazzi, S., 2012. The effect of wind waves on the development of river mouth bars, *Geophysical Research Letters*, 39, L12607.

Nienhuis, J.H.; Ashton, A.D.; Nardin, W.; Fagherazzi, S., and Giosan, L., 2016. Alongshore sediment bypassing as a control on river mouth morphodynamics. *Journal of Geophysical Research: Earth Surface*, 121, 664–683.

NOAA (National Oceanic and Atmospheric Administration), 2017. WaveWatch III - Marine Modeling and Analysis Branch, http://polar.ncep.noaa.gov/waves/index2.shtml

Pelnard-Considère, R., 1956. Essai de theorie de l'evolution des formes de rivage en plages de sable et de galets (in French). In *4th Journees de l'Hydraulique, Les Energies de la Mer*, vol. 3, pp. 289–298.

Pinto, L; Fortunato, A.B.; Zhang, Y.; Oliveira, A., and Sancho, F.E.P., 2012. Development and validation of a three-dimensional morphodynamic modelling system for non-cohesive sediments. *Ocean Modelling*, 57–58, 1–14.

Roelvink, D., and Reniers, A., 2011. *A guide to modeling coastal morphology*. Singapore: World Scientific, 274p.

Sao, N.T.; Huan, N.M.; Tuan, N.C., and Kha, D.D., 2010. Variations of sediment and morphology changes in Cua Tung beach and adjacent region, Quang Tri province (in Vietnamese). *VNU Journal of Science: Natural Sciences and Technology*, 26(3S), 427–434.

Schoonees, J.S., and Theron, A.K., 1996. Improvement of the most accurate longshore transport formula. In *Proceedings of the 25th International Conference on Coastal Engineering*, Orlando, FL, USA, pp. 3652–3664.

Soulsby, R., 1997. *Dynamics of Marine Sands*, London: Thomas Telford, 249p.

Tien, T.Q., 2004. Use of hindcast wave field by WAM model for calculation of sediment transport in littoral zone of Vietnam Central. In: Proceedings of the 14th OMISAR Workshop on Ocean Models, Taipei, Taiwan.

Van Rijn, L.C., 2014. A simple general expression for longshore transport of sand, gravel and shingle. *Coastal Engineering*, 90, 23–39.

Warner, J.C.; Sherwood, C.R.; Signell, R.P.; Harris, C.K., and Arango, H.G., 2008. Development of a three-dimensional, regional, coupled wave, current, and sediment-transport model. *Computers & Geosciences*, 34, 1284–1306.

Weatherall, P.; Marks, K.M.; Jakobsson, M.; Schmitt, T.; Tani, S.; Arndt, J.E.; Rovere, M.; Chayes, D.; Ferrini, V., and Wigley, R., 2015. A new digital bathymetric model of the world's oceans. *Earth and Space Science*, 2, 331–345.

Woodroffe, C.D., 2002. *Coasts: Form, Process and Evolution*, Cambridge University Press, 623p.

Wright, L.D., 1977. Sediment transport and deposition at river mouths: A synthesis. *Geological Society of America Bulletin*, 88(6), 857–868.

Wright, L.D., and Short, A.D., 1984. Morphodynamics variability of surf zones and beaches: a synthesis. *Marine Geology*, 56, 93–118.